The Open and Closed Forms of a Perfluoro Diarylethene Photoswitch─Halogen Bonding, Network Topology, and CSD Analysis

Downloaded from: https://research.chalmers.se, 2026-04-06 14:26 UTC

Citation for the original published paper (version of record):
Öhrström, L., Andreasson, J., Li, H. et al (2024). The Open and Closed Forms of a Perfluoro Diarylethene Photoswitch─Halogen Bonding, Network Topology, and CSD Analysis. Crystal Growth & Design, 24(3): 923-931.
http://dx.doi.org/10.1021/acs.cgd.3c00767

N.B. When citing this work, cite the original published paper.

research.chalmers.se offers the possibility of retrieving research publications produced at Chalmers University of Technology. It covers all kind of research output: articles, dissertations, conference papers, reports etc. since 2004. research.chalmers.se is administrated and maintained by Chalmers Library

(article starts on next page)

CRYSTAL GROWTH & DESIGN

pubs.acs.org/crystal

Article

Open Access

This article is licensed under CC-BY 4.0

The Open and Closed Forms of a Perfluoro Diarylethene Photoswitch—Halogen Bonding, Network Topology, and CSD Analysis

Lars Öhrström,* Joakim Andréasson, Hao Li, and Francoise M. Amombo Noa*

Cite This: *Cryst. Growth Des.* 2024, 24, 923–931

Read Online

ACCESS | Metrics & More | Article Recommendations | Supporting Information

ABSTRACT: The structure of the perfluoro cyclopentene diarylethene photoswitch 3,3′-(perfluorocyclopent-1-ene-1,2-diyl)bis(2-ethyl-6-iodobenzo[*b*]thiophene 1,1-dioxide) ($C_{25}H_{16}F_6I_2O_4S_2$) **1** at 100 K has a tetragonal ($I4_1/a$) symmetry. The compound has a halogen-bonded network structure described by the uninodal five-connected **joa** net. This net is related to another uninodal six-connected net **sfo**. Analysis using the Cambridge Structural Database (CSD) shows that the majority of structures with the perfluoro cyclopentene diarylethene motif, >85%, have a C···C distance of around 3.5 Å where a new single bond will develop during photoswitching, whereas compound **1** falls in a second smaller category with C···C distances of around 4.2 Å. The photochemical reaction of **1** under UV light in ethanol gave a closed form that crystallized as ethanol solvate **2a** in the $P2_1/c$ space group, and recrystallization in acetone gave the nonsolvated form **2b** crystallizing in the space group *Fdd*2. We did not observe, and do not believe that it is possible, to photoswitch **1** in the solid state as the C···C distance where a new single bond will develop is very long.

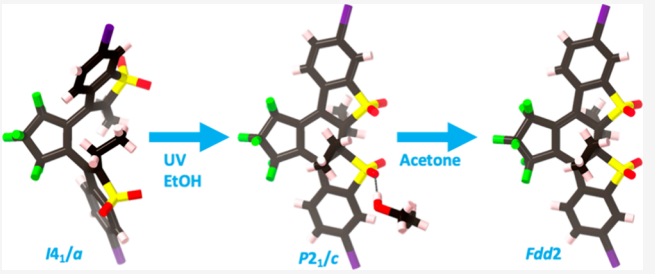

INTRODUCTION

Diarylethene (DAE) photoswitches are identified as one of the prime families of photochromic materials.[1] Since their serendipitous discovery in 1988,[2] demonstrations of DAE applicability have been made over an impressive range of research disciplines, including chemistry,[3−5] nanotechnology,[6−10] life science,[11−15] materials science,[16−18] and information processing.[19−21] One of the reasons for the versatility of these photoswitches is the possibility of specific applications by introducing substituents of varying kinds to tailor-make the physicochemical properties while maintaining the photochromic behavior: the high thermal stability of both isomeric forms, excellent photostability, and the possibility of highly enriching both isomeric forms by light exposure. Moreover, a subset of DAEs displays very intense emission only in one of the two isomeric forms,[22,23] which is a sought-after property in the design of fluorescent materials.

About 600 structures of open forms are known in the Cambridge Structural Database (CSD),[24] whereas closed forms are known in only about 60 cases, most of these with disorder or other crystallographic problems likely arising from their photochemical preparations, back-isomerization to the open isomeric form during lengthy crystallization, or instability of the closed form in an X-ray beam.[25]

Herein, we describe the crystal growth and structures to a high precision of the open **1** and closed **2a** and **2b** forms of such a derivative, DAEg (3,3′-(perfluorocyclopent-1-ene-1,2-diyl)bis(2-ethyl-6-iodobenzo[*b*]thiophene 1,1-dioxide). This is the green part of an all-photonic full color RGB system,[26] symmetrically decorated with iodine atoms to allow for the formation of halogen-bonded network. The intermolecular interactions are shown to be substantially different in all three forms.

The distinct parts of these molecules will make many different intermolecular forces compete, such as homo- and hetero-halogen···halogen bonding, weak hydrogen bonding, and potentially also $\pi-\pi$ stacking. To evaluate their different impact, it is valuable to have examples with very similar or identical molecules to study, especially as the halogen···halogen interaction is still a matter of some debate.[27−29]

Compounds with C−F bonds among these intermolecular interactions are important for two reasons. First, the increasing number of C−F-containing pharmaceuticals[30] makes crystal engineering with this type of compound more important in tailoring their properties in a drug formulation. Second, the removal of per- and polyfluoroalkyl substances (PFASs) in drinking water treatment is still very much a problem,[31] and

Received: June 26, 2023
Revised: January 9, 2024
Accepted: January 9, 2024
Published: January 25, 2024

Downloaded via CHALMERS UNIV OF TECHNOLOGY on February 23, 2024 at 13:40:07 (UTC).
See https://pubs.acs.org/sharingguidelines for options on how to legitimately share published articles.

ACS Publications

© 2024 The Authors. Published by American Chemical Society

https://doi.org/10.1021/acs.cgd.3c00767
Cryst. Growth Des. 2024, 24, 923−931

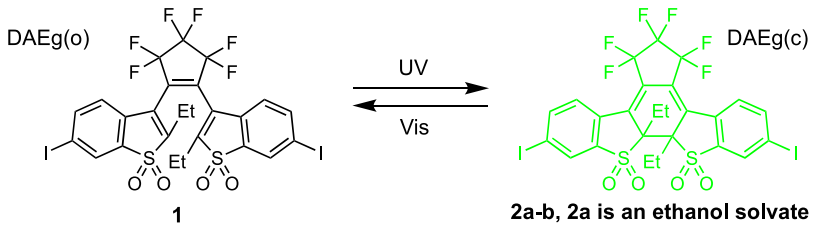

Figure 1. Photoswitching response of the fluorescent DAEg. We present the crystal growth and structures of the open form **1** and two crystal varieties of the closed form, **2a** and **2b**.

Table 1. Crystallographic Data and Structure Refinement Parameters for 1, 2a, and 2b

	1	2a	2b
formula	$C_{25}H_{16}F_6I_2O_4S_2$	$C_{25}H_{16}F_6I_2O_4S_2{\cdot}C_2H_6O$	$C_{25}H_{16}F_6I_2O_4S_2$
M_r	812.30	858.36	812.30
crystal system	tetragonal	monoclinic	orthorhombic
space group	$I4_1/a$	$P2_1/c$	$Fdd2$
temperature (K)	100.0 (1)	119 (2)	112.2 (2)
a (Å)	34.1082 (3)	8.0302 (1)	51.7499 (6)
b (Å)	34.1082 (3)	22.7905 (3)	25.0685 (2)
c (Å)	9.35233 (10)	15.8993 (2)	8.27894 (8)
α (°)	90	90	90
β (°)	90	99.053 (1)	90
γ (°)	90	90	90
V (Å^3)	10880.2 (2)	2873.52 (6)	10740.18 (19)
Z	16	4	16
Dx (Mg m^{-3})	1.984	1.984	2.009
μ (mm^{-1})	20.27	19.25	20.53
crystal size (mm)	0.21 × 0.06 × 0.05	0.07 × 0.06 × 0.05	0.11 × 0.10 × 0.06
T_{min}, T_{max}	0.845, 1.000	0.406, 0.578	0.737, 0.920
measured, independent, and observed $[I > 2\sigma(I)]$ reflections	30405, 5762, 5298	27611, 5763, 5428	49983, 5424, 5398
R_{int}	0.034	0.032	0.034
$R[F^2 > 2\sigma(F^2)]$ $wR(F^2)$	R_1= 0.029, wR_1= 0.069	R_1= 0.023, wR_1= 0.053	R_1= 0.023, wR_1= 0.062
GOF	1.06	1.05	1.04
no. of reflections	5762	5763	5424
no. of parameters	354	386	354
$\Delta\rho_{max}$, $\Delta\rho_{min}$ (e Å^{-3})	0.94, −0.79	0.66, −0.57	0.84, −0.76
Flack parameter			−0.007 (4)
CCDC no.	2242050	2266015	2266016

intermolecular interactions that could be built into a filter device to selectively pick up PFAS molecules could be a viable approach. In general, halogen bonding in cocrystals of open perfluoro cyclopentene DAEs has yielded porous structures responsive to various stimuli,[32,33] and halogen-bonded photoresponsive systems based on other chromophores were reported by Resnati et al.[34,35]

The present study investigates crystals obtained from irradiation experiments in solution and their intermolecular interactions. The solid-phase conversion and interconversion of these phases, if possible, are other matters that we plan to address in a future study.

EXPERIMENTAL PART

Materials and Physical Measurements. The parent open form DAEg(o) **1** was prepared as described previously[22] and was obtained as a yellow solid with melting points between 213 and 214 °C using a Gallenkamp melting point instrument and between 210 and 212 °C by TGA/DSC (Mettler Toledo TGA/DSC 3$^+$, Figure S7). The acetone and ethanol used were of analytical grade. For ring closure experiments, 3 mg of **1** was dissolved in 3 mL of solvent and UV irradiation was performed with a UMV-57 UV lamp at 302 nm, from Analytik Jena, Upland, CA, United States, for 1 h. Slow evaporation at 20 °C for 2−5 days followed by crystal growth at 7 °C gave suitable crystals for structure determination. The closed form of **2a**, an ethanol solvate, was prepared by dissolving **1** in ethanol and irradiating with UV light at 302 nm. Subsequent slow evaporation at 7 °C gave crystals of **2a** mixed with crystals of **2b** and **1**. Room-temperature evaporation of the ethanol solution followed by reirradiation and recrystallization in acetone at 7 °C gave crystals of the nonsolvated closed form **2b**. Compound **2b** is an amber solid with melting points of 230−232 °C (with simultaneous decomposition) by using a melting point instrument and 228−230 °C by DSC (Figure S7).

Irradiation of open form crystals **1** in the solid state produced no changes in these crystals.

Crystal data collection and structure refinement details are summarized in Table 1. Suitable single crystals of the three forms were mounted on Hampton loops or MiTeGen mounts. Data were collected using an XtaLAB Synergy-R HyPix diffractometer operating at 100 K for **1**, 119 K for **2a**, and 112 K for **2b** for the single-crystal measurements and at 278 K for the powder diffraction measurements.

Single-crystal data were measured using ω scans of 0.5° per frame using Cu Kα radiation. The diffraction pattern was indexed, and the total number of runs and images was based on the strategy calculation from the program CrysAlisPro,[36] and the unit cell was refined using CrysAlisPro.[36]

Data reduction, scaling, and absorption corrections were performed using CrysAlisPro.[36] A Gaussian absorption correction was performed

https://doi.org/10.1021/acs.cgd.3c00767
Cryst. Growth Des. 2024, 24, 923−931

using CrysAlisPro.[36] Numerical absorption correction was based on a Gaussian integration over a multifaceted crystal model, and empirical absorption correction was performed using spherical harmonics, as implemented in the SCALE3 ABSPACK scaling algorithm.

Structures were solved by the SHELXT[37] structure solution program using Intrinsic Phasing and refined by Least Squares using version 2016/6 of SHELXL 2016/6.[37] All nonhydrogen atoms were refined anisotropically. Hydrogen atom positions were calculated geometrically and refined using the riding model, except for the hydrogen atom of the ethanol hydroxyl group in **2a** that was localized from the difference density map and its position refined.

Powder X-ray diffraction (PXRD) measurements were carried out at 278 K using a Rigaku Synergy-R X-ray diffractometer with Cu Kα radiation.

Cambridge Structural Database. CSD version 5.44 (April 2023) was used for all ConQuest searches. For statistical runs, only organic structures without disorder and with an *R* factor less than 10% were selected. The suitable crystal structures were analyzed with the Mercury 2023.1.0 software. Aromatic iodine structures were searched by using two linear three-atom units (connected by aromatic bonds where the central atom is a carbon with an iodine substituent and the two other atoms are any nonmetal (X−C(I)−X with X = any nonmetal and "−" an aromatic bond). Intermolecular I···I distances of up to 5 Å were then selected to make sure that we cover all cases, although 5 Å is very long. The total number of hits for this search was 3810.

RESULTS AND DISCUSSION

The parent open form DAEg(o) compound **1** was prepared according to the literature[22] and recrystallized from dimethylformamide. The closed form **2a**, an ethanol solvate, was prepared by dissolving **1** in ethanol and irradiating with UV light at 302 nm. Subsequent slow evaporation at 7 °C gave crystals of **2a** and recovered starting material. Room-temperature evaporation of the ethanol solution followed by recrystallization and reirradiation in acetone gave crystals of the nonsolvated closed form **2b** after crystal growth at 7 °C. PXRD and TGA/DCS data of **1** and **2b** are presented in the Supporting Information (SI).

The completeness of the photochemical conversion was confirmed by UV−vis spectroscopy (see Figure 2), but as the crystallization was ongoing for several days, some thermal reversion to the open form could be detected. This was done by accidentally picking crystals of the open form **1** in the closed form preparations and detecting the unit cell of **1** during crystal screening. This easily happens because the three crystal forms have similar yellow colors (in the bulk **1** is a clearer yellow and **2b** is more amber) and morphology. We also needed to grow relatively large crystals for the closed forms **2a** and **2b** to minimize the measuring time. The reason was because the samples tended to lose crystallinity after 2−3 h in the X-ray beam.

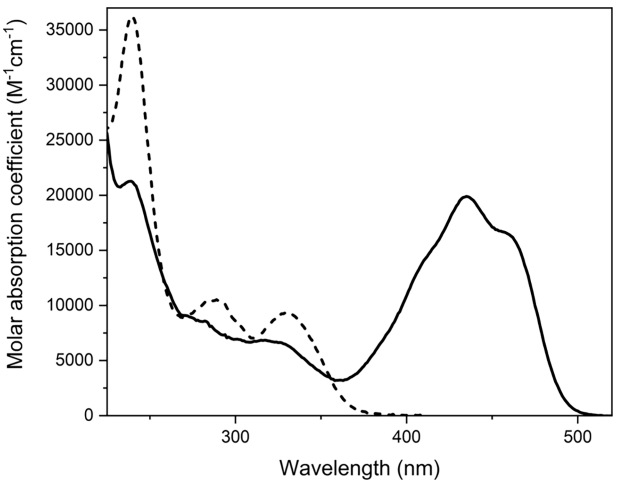

Figure 2. Solution UV−vis spectra of the open form **1** (dotted) and the closed form **2** (solid) in acetonitrile.

The van der Waals radii of Bondi[38] were employed to estimate the halogen···halogen (X···X) interactions in different compounds, and the relevant distances are recorded in Table 2

Table 2. X···X Interactions in 1, 2a, and 2b[a]

compound	X···X	d (Å)	d − Σvdw (Å)	%	$\theta_2 - \theta_1$(°)
1	$I_{24}\cdots I_{24}$	4.131(1)	+0.17	+4.3	46.93(8)
	$I_{24}\cdots I_{35}$	4.032(1)	+0.07	+1.8	48.14(8)
	$I_{35}\cdots I_{35}$	4.115(1)	+0.15	+3.9	47.13(8)
	$I_{24}\cdots I_{35}$	4.220(1)	+0.26	+6.5	64.28(8)
	$F_{31}\cdots F_{34}$	2.833(1)	−0.11	−3.6	
2a	$F_{34}\cdots F_{35}$	3.001(1)	+0.06	+2.1	
	$F_{38}\cdots F_{39}$	2.778(1)	−0.16	−5.5	
	$I_{29}\cdots F_{39}$	3.695(3)	+0.24	+7.0	31.37(7)
	$I_{29}\cdots F_{38}$	3.746(3)	+0.29	+8.4	24.37(7)
2b	$I_{17}\cdots I_{28}$	4.112(1)	+0.15	+3.8	39.50(1)
	$F_{34}\cdots F_{36}$	3.116(1)	+0.18	+6.0	
	$F_{34}\cdots F_{37}$	2.881(1)	−0.06	−2.0	
	$I_{29}\cdots F_{39}$	3.817(3)	+0.36	+10.6	81.8(3)

[a]For iodine, we also list the C−I···X-C angle differences $\theta_2 - \theta_1$.

if they were less than the sum of the van der Waals radii + 10% (this we note is already long, but estimates of these radii may differ a couple of percent units). Tables S1−S3 in the SI list other types of interactions that do contribute to the stabilization of various structures.

Structure of DAEg(o) 1. Crystallographic data are presented in Table 1. The open form **1** crystallizes in the space group $I4_1/a$ with $Z = 16$. The structure has interactions such as C−H···O and C−H···F and is further stabilized with C−F···π and S−O···π, showing shortest distances at 3.001(1) and 3.472(1) Å, respectively. The molecular structure (Figure 3) is unremarkable except for the distance between the alkyl-substituted carbons. In this case, C1−C15 is at 4.290(4) Å, where the new single bond will develop in the closed form.

The photoswitching properties in the solid state are probably dependent on the distance between the alkyl-substituted carbons, in this case C1 and C15, 4.290(4) Å, and it has been suggested that this distance needs to be shorter than 3.5 Å for solid state photoswitching to be viable. Indeed, irradiation of open form crystals **1** in the solid state produced no changes in these crystals.

Surveying the CSD[24] for similar structures reveals two distinct conformational spaces dependent on the torsion angle between the ethene unit and the alkyl-substituted carbon; see Figure 4 (this is more or less the only degree of freedom that these molecules have). The majority of structures, >85%, have a C···C distance of around 3.5 Å, whereas **1** falls in the category with a smaller number-of-hits maximum around 4.2 Å. The reason for this correlation is obscure but may be related to steric crowding around these carbons. It would be useful to be able to design this distance to be short, as this would imply a handle on controlling the mechanochemical properties of these crystals.[39]

https://doi.org/10.1021/acs.cgd.3c00767
Cryst. Growth Des. 2024, 24, 923−931

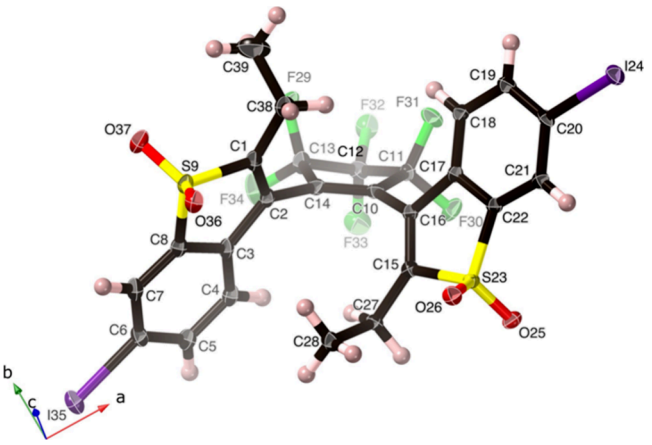

Figure 3. Molecular structure of DAEg(o) **1**. Displacement ellipsoids are drawn at the 50% probability level. We do not expect or indeed observe any photoswitching in the solid state (Figure 1) as the distance between C1 and C15, 4.290(4) Å, is much longer than the suggested limit of 3.5 Å. See also Figure 4.

The solid state packing of **1** is directed by halogen···halogen bonds[40] extending the molecular structure to a network in three dimensions. The analysis of such compounds by the unifying concept of network topology has greatly helped our understanding and description of such diverse materials as allotropes of elements, metal−organic frameworks, and ice polymorphs,[41] but examples with halogen···halogen bonds are still rare.[42] Moreover, the description of new nets, especially if they are uninodal (only one kind of vertex in the asymmetric unit of the most symmetric embedding), adds value to the entire field. We will see here how two new nets emerging from the structural description of **1** are relevant to the large class of metal−organic frameworks known as rod-MOFs.[43]

Although these halogen···halogen interactions are not as strong as the "activated" N···I or I···I interactions, where one frequently sees intermolecular atom···atom distances on the order of 75% of the sum of the van der Waals (vdW) radii,[42] an analysis of organic structures with aromatic iodines in the CSD reveals an attractive interaction as the structures versus I···I distance plot has a clear maximum (corresponding to a minimum in the potential energy) (see Figure 5, left).

We can even observe a hint of two types of preferred distances, something to be expected if the interaction conforms to what has been found for the stronger halogen bonds. Indeed, in the right graph, absolute values of the C−I···I angle differences $\theta_2 - \theta_1$[44] are used as an additional parameter; two distinct areas can be perceived in the heat plot. These angles correspond to the classification of the halogen···halogen interactions into two types: a longer type I where the two C−I···I angles are roughly the same and a stronger type II where the angles come close to 90 and 180°.[44] In Figure 5 right, we see the type II interactions for short distances, just around the sum of the vdW radii for I (4.08 Å) and angle differences from 40° and up. We also indicate the values found for **1** by black circles in the right graph. (The values for the four shorter interactions in **1** are 4.032(1) Å, 155.58(8)°, 107.44(8)°; 4.115(1) Å, 133.25(8)°, 86.12(8)°; 4.131(1) Å, 146.6(8)°, 99.67(8)°; and 4.220(1) Å, 137.76(8)°, 73.48(8)°.)

These I···I interactions form chains, or rods, along the *c* axis (see Figure 6). Each iodine has four type II interactions, and while these are somewhat fluid in their interangle dependence, they may still be structure directing. Overall, this results in a 3D network where the rods are connected by perfluorocyclopent-1-ene-diaryl linkers and here the network is emphasized in purple; see Figure 6.

This motif of interconnected rods with parallel channels is familiar to anyone interested in the structure and topology analysis of metal−organic frameworks, where such compounds go under the name "rod-MOFs".[43] The network analysis of these materials is important from both a description and a synthesis planning perspective and has recently been debated.[43,45−47]

Taking the type II interactions into account, every iodine atom can be assigned as a five-connected node (or vertex) and the topology analyzed using SYSTRE.[48] The most symmetric form (embedding) of the so-formed **joa** net is displayed in Figure 7, left. The **joa** net is uninodal (one kind of vertex) with four different links (edges; the edge transitivity of this net is thus 4) and a point symbol $\{4^7.6^3\}$ signifying that it contains four rings and six rings (the superscripts sum to the number of possible link pairs emerging from a node), and it has not previously been described.

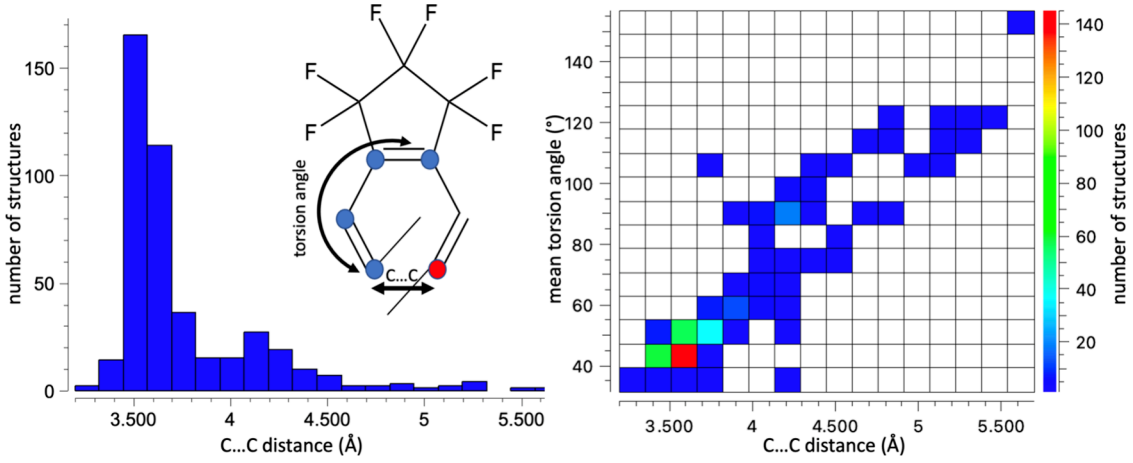

Figure 4. Analysis of structures from the CSD for perfluorocyclopent-1-ene-diaryl derivatives reveals two distinct conformational spaces dependent on the torsion angle between the ethene unit and the alkyl-substituted carbon. DAEg(o) **1** has a C···C distance of 4.290(4) Å and torsion angles of 73.8(4) and 66.2(4)°, conforming to these data.

https://doi.org/10.1021/acs.cgd.3c00767
Cryst. Growth Des. 2024, 24, 923−931

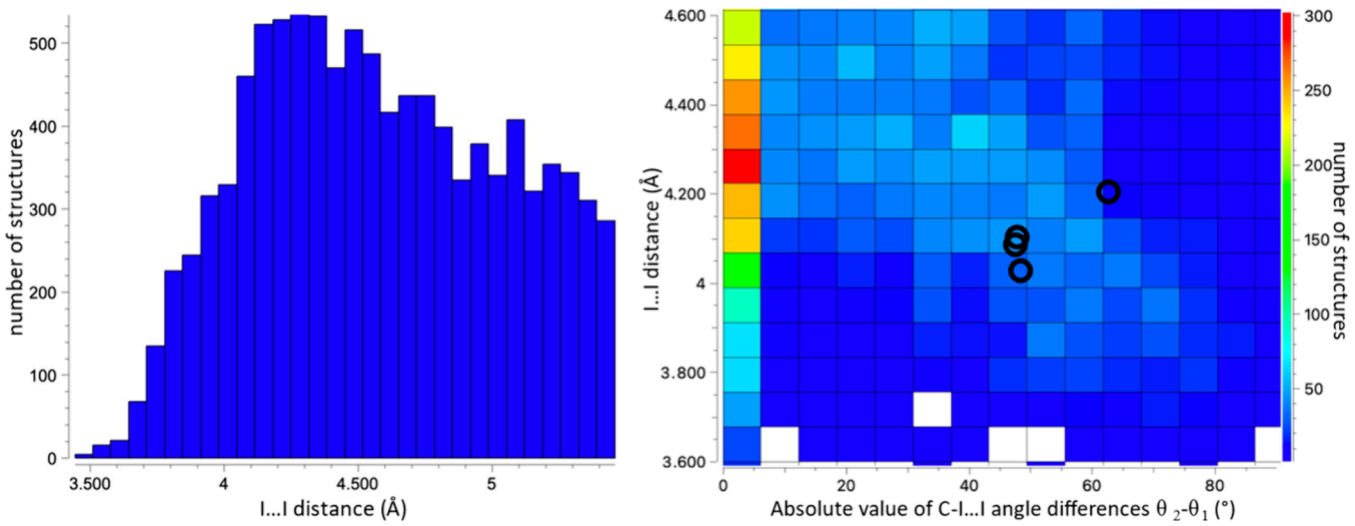

Figure 5. Analysis of organic structures of aromatic iodines in the CSD. The hint of two types of distances that may be inferred from the left graph is clearly displayed in the right graph, where the absolute values of the C−I···I angle differences $\theta_2 - \theta_1$[44] are used as an additional parameter. These regions correspond to type I ($\theta_2 = \theta_1$) and type II ($\theta_2 \approx 180°$, $\theta_1 \approx 90°$) halogen···halogen interactions. Black circles refer to **1**.

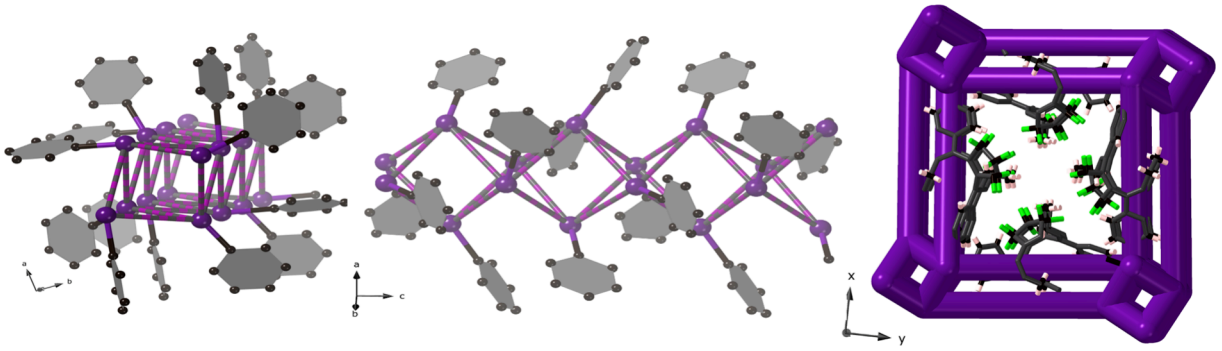

Figure 6. Left and middle: The I···I interactions form chains or rods along the *c* axis, in **1**. Right: Overall, this results in a 3D network where the rods are connected by perfluoro DAE linkers and here the network is emphasized in purple.

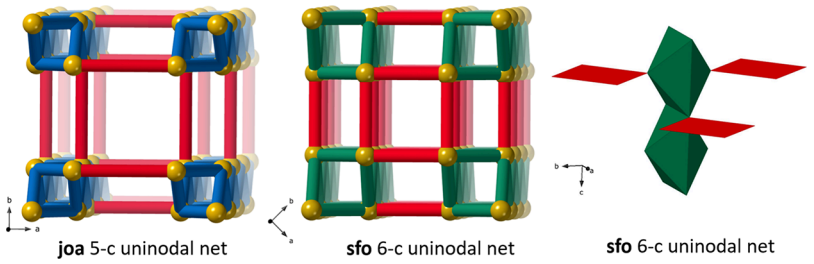

Figure 7. Left: most symmetric form of the uninodal (one kind of vertex) five-connected **joa** net describing DAEg(o) **1**. The red links correspond to the perfluorocyclopentene DAE, and the blue links correspond to the halogen-bonded rods. The edge transitivity of this net is 4. Middle: Adding a link to this net, making another connection between the rods, results in the six-connected uninodal **sfo** net with edge transitivity 2. Right: squares and flattened octahedra visible in the most symmetric form of this net.

Inspecting the **joa** net, we observed that a six-connected network could easily be constructed by adding one set of linkers; see Figure 7, right. We initially suspected that this would be a known net and that the **joa** net thus could be easily derived from an existing net. However, the topology analysis revealed this to be yet another unknown net, again uninodal but with only two types of links and the point symbol $\{4^{11}.6^4\}$. In view of the squares and flattened octahedra visible in the most symmetric form (Figure 6, right), this net is called **sfo**.

Structures of DAEg(c)·EtOH 2a and DAEg(c) 2b. Crystallographic data are presented in Table 1. Compound **2a** crystallizes in $P2_1/c$ with $Z = 4$. The asymmetric unit contains one molecule of the closed form and an ethanol solvent. There are no I···I interactions but two F···F (see Table 2); the reason is that the structure is strongly governed by O−H···O, C−H···O, and C−H···F interactions. Some weaker interactions like C−H···π, C−I···π, and S−O···π are also observed with the shortest distances at 2.068(1), 3.720(1), and 3.822(1) Å, respectively. The ethanol molecule hydrogen bonds to O31 in the closed form as indicated in Figure 8 (O···H: 2.08(5)°; O···O: 2.894(3)°; O−H···O 168(5)°) but has no other significant interactions.

https://doi.org/10.1021/acs.cgd.3c00767
Cryst. Growth Des. 2024, 24, 923−931

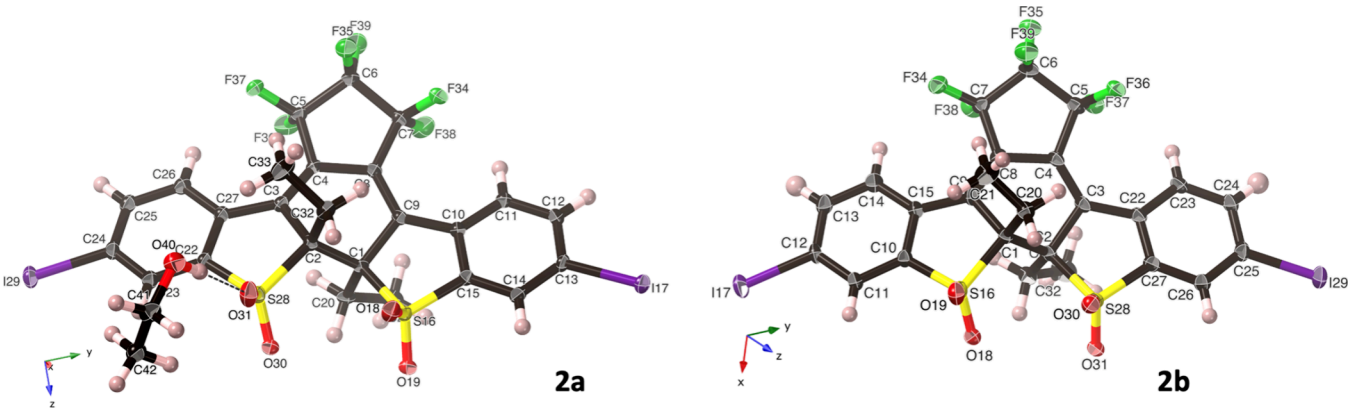

Figure 8. Molecular structures of DAEg(c)·EtOH **2a** and DAEg(c) **2b**. Displacement ellipsoids are drawn at the 50% probability level.

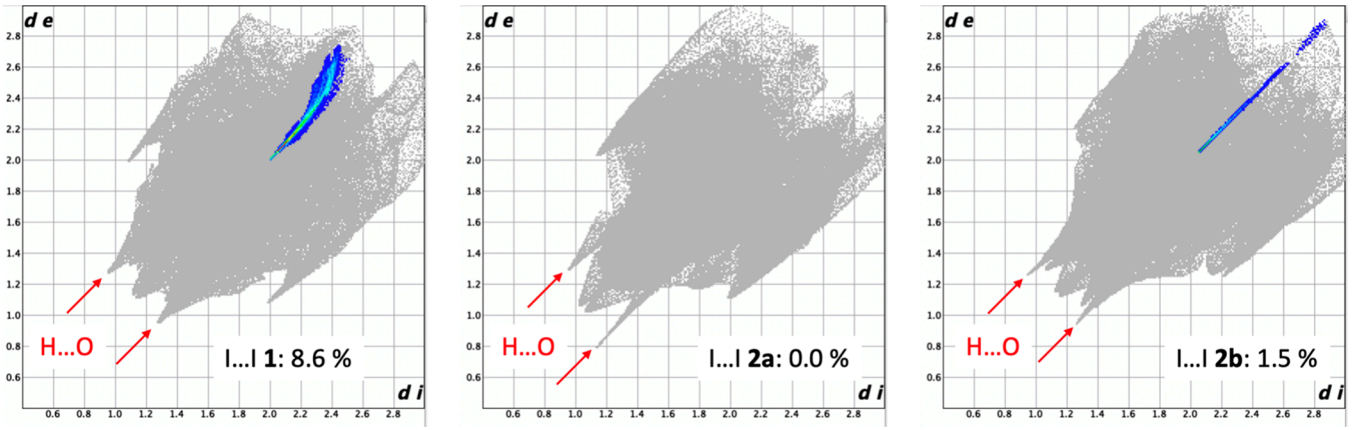

Figure 9. Hirshfeld surface analysis,[49] with the so-called fingerprint plots. The gray areas show the total interaction plot, and in color, the specific interaction is highlighted with its percent contribution to the surface. In this case, we look at the I···I interactions. Arrows indicate O···H interactions, similar in the three compounds except for the extra ethanol hydrogen bonding visible for **2a**, making these peaks unsymmetric.

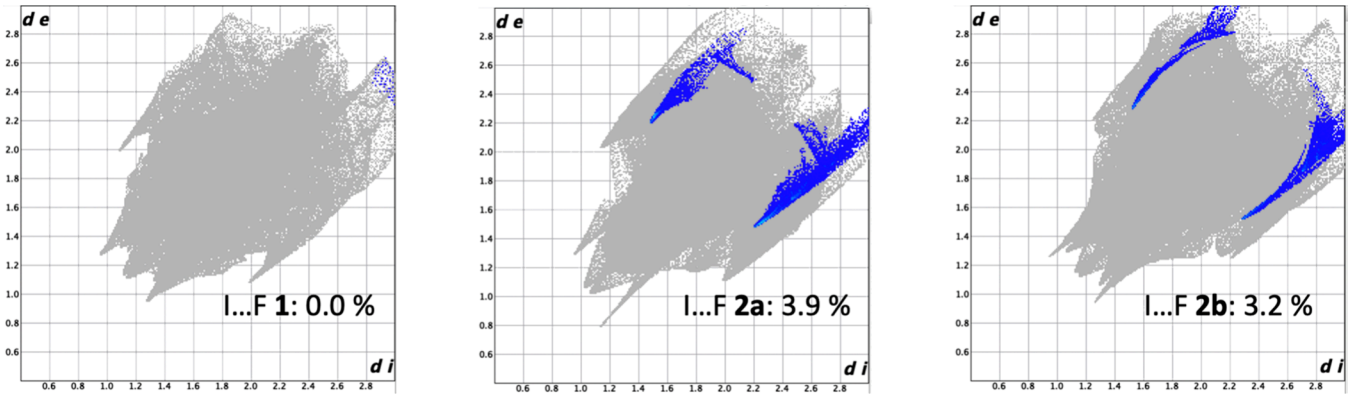

Figure 10. Hirshfeld surface analysis,[49] with fingerprint plots. The gray areas show the total interaction plot, and in color, the I···F interactions are highlighted with their percentage contributions to the total surface.

On the other hand, the nonsolvated closed form **2b** was solved in *Fdd*2 with $Z = 16$. There is only one molecule of **2b** in the asymmetric unit. It contains interactions such as C−H···O and C−H···F, which are dominant in the structure and further stabilize with C−H···π and C−F···π (2.600(1) and 3.526(1) Å, respectively). The molecular structures (Figure 8) are unremarkable and identical for the DAEg(c) unit in the two cases, all the way to the hydrogen positions on the ethyl groups (overlap RMSD 0.173, max D 0.469 as calculated by Mercury; see also Figure S1).

The intermolecular interactions are, on the other hand, very different. Besides the obvious hydrogen-bonding interactions, there are a few features that differentiate the three compounds in this study. We do so by using Hirshfeld surface analysis,[49] and the most pertinent results are shown as the so-called fingerprint plots where individual atom−atom interactions have been selected and are shown in Figure 9 (additional plots can be found in Figures S2−S4 in the SI).

First, we note the different I···I interactions in these three structures.

https://doi.org/10.1021/acs.cgd.3c00767
Cryst. Growth Des. 2024, 24, 923−931

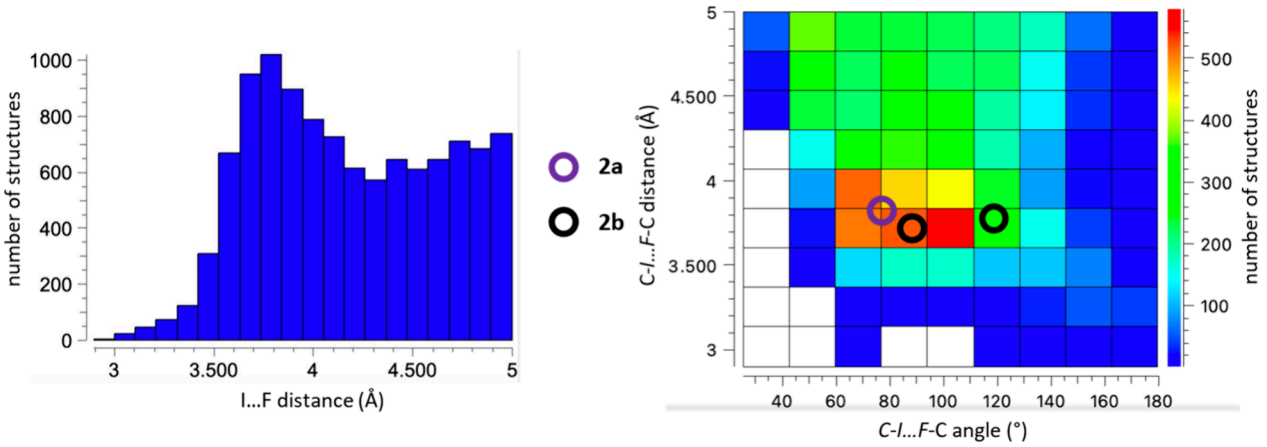

Figure 11. Analysis of the organic structures containing C−I and C−F units in the CSD. A clear maximum in the histogram on the left side indicates an attractive interaction, and in the right graph, we see how it also correlates to the C−I···F angle. Violet circles refer to measured values for **2a,** and black circles to values for **2b**.

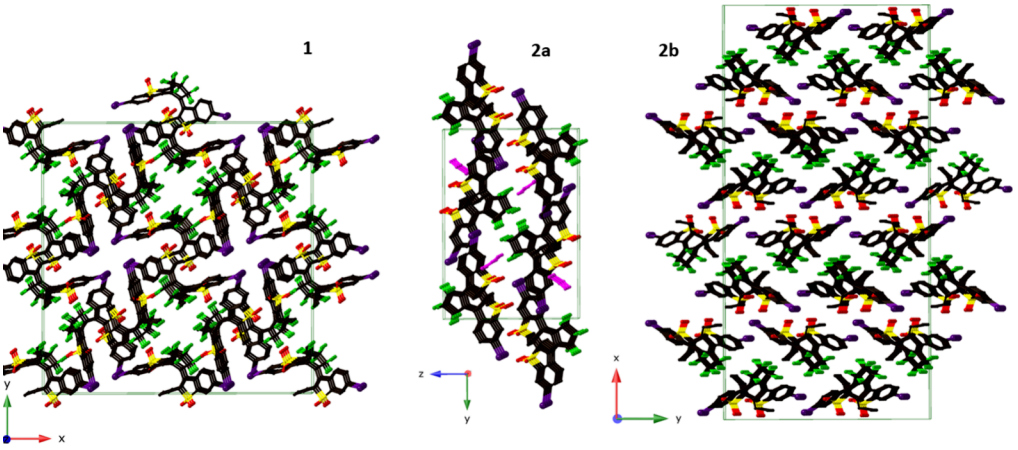

Figure 12. Packing diagrams for DAEg(o) **1** and DAEg(c) **2a** (with the ethanol molecules in pink) and **2b** project along the shortest unit cell axis for each structure.

It is clear from Figure 9 that the I···I interaction is only prominent and possibly structure directing in open form **1**. H···O interactions (19.4, 19.1, and 11.7%, respectively) are of course prominent in all structures and are also pointed out in Figure 9. H···H contacts (16.2, 21.3, and 17.9%, respectively) may be repulsive or attractive in nature[50] (we see no tendencies of a preferred intermolecular distance in the CSD; see Figure S5), and the same may be true for the F···F (5.8, 6, and 2.8%, respectively) although a preferred intermolecular distance can be seen in analysis of the CSD (see Figure S5). Despite the aromatic rings present in the structure, we see no signs of $\pi-\pi$ stacking, and the C···C contacts are negligible (1.0, 1.6, and 0.5%). The F···H contacts (16.0, 15.1, and 23.6%, respectively) may indicate some weak hydrogen bonds, but what also stand out in a comparison are the I···F interactions (0.0, 3.9, and 3.2%, respectively) (see Figure 10), specifically their absence in **1** and the marked pointed maxima in **2a** and **2b**.

Additional Hirshfeld fingerprint plots are found in the SI.

If we look at intermolecular C−I···F−C distances and C−I···F angles in the CSD, we see a maximum number of hits at 3.6−3.8 Å, which indicates that this is a preferred I···F distance, suggesting that the I···F interaction is of attractive nature around this distance and in the region 80−100° (Figure 11). This broadly corresponds to the shortest I···F distances in **2a** and **2b**, which are also indicated in the figure.

Packing diagrams of **1**, **2a**, and **2b** are given in Figure 12, where some of the discussion above can be traced. It is difficult to pinpoint any individual interaction as the structure-directing agent, and the existence of two distinct crystal forms of DAEg(c) **2** indicates that this is a delicate balance between a number of factors.

CONCLUSIONS

This type of DAE photoswitch has only one degree of freedom, and it should be possible to design, maybe with the help of computational simulations, similar compounds that can undergo the photoswitching reaction also in the solid state. We have also identified several intermolecular interactions that may be important for the structures of both the open and closed forms of DAEs. Among these, the halogen···halogen interactions seem the most important from a practical point of view, although none of these individual interactions can be singled out as dominant, as all three forms display very different contributions in their crystal structures. Nevertheless, we have shown that halogen···halogen interactions are important interactions in all these structures and can contribute to the crystal engineering design of photoswitching molecules.

https://doi.org/10.1021/acs.cgd.3c00767
Cryst. Growth Des. 2024, 24, 923−931

■ ASSOCIATED CONTENT

Supporting Information

The Supporting Information is available free of charge at https://pubs.acs.org/doi/10.1021/acs.cgd.3c00767.

Tables of hydrogen bonding and short intermolecular contacts, overlay plots of **2a** and **2b**, additional fingerprint plots, and details of the CSD searches, powder diffractograms, thermogravimetric analysis, and network topology analysis (PDF)

Accession Codes

Accession codes CCDC 2242050, 2266015, and 2266016 contain the supplementary crystallographic data for this paper. These data can be obtained free of charge via www.ccdc.cam.ac.uk/data_request/cif, by emailing data_request@ccdc.cam.ac.uk, or by contacting The Cambridge Crystallographic Data Centre, 12 Union Road, Cambridge CB2 1EZ, UK; fax: +44 1223 336033.

■ AUTHOR INFORMATION

Corresponding Authors

Lars Öhrström − *Department of Chemistry and Chemical Engineering, Chalmers University of Technology, Gothenburg 412 96, Sweden;* orcid.org/0000-0002-6420-2141; Email: ohrstrom@chalmers.se

Francoise M. Amombo Noa − *Department of Chemistry and Chemical Engineering, Chalmers University of Technology, Gothenburg 412 96, Sweden;* orcid.org/0000-0001-8361-3432; Email: mystere@chalmers.se

Authors

Joakim Andréasson − *Department of Chemistry and Chemical Engineering, Chalmers University of Technology, Gothenburg 412 96, Sweden;* orcid.org/0000-0003-4695-7943

Hao Li − *Department of Chemistry and Chemical Engineering, Chalmers University of Technology, Gothenburg 412 96, Sweden*

Complete contact information is available at: https://pubs.acs.org/10.1021/acs.cgd.3c00767

Notes

The authors declare no competing financial interest.

■ ACKNOWLEDGMENTS

We thank the Swedish Research Council (F.M.A.N., L.Ö.), the Swedish Research Council for Sustainable Development FORMAS (H.L.), the Olle Engkvist Foundation (F.M.A.N., L.Ö.), and the Chalmers Areas of Advance Energy, Materials, Health and Nano (F.M.A.N.) for funding. We also acknowledge the Chalmers Materials Analysis Laboratory and thank Prof. Michael O'Keeffe for adding the **joa** and **sfo** nets to the Reticular Chemistry Structural Resource database.

■ REFERENCES

(1) Irie, M.; Fulcaminato, T.; Matsuda, K.; Kobatake, S. Photochromism of Diarylethene Molecules and Crystals: Memories, Switches, and Actuators. *Chem. Rev.* **2014**, *114* (24), 12174−12277.

(2) Irie, M.; Mohri, M. Thermally irreversible photochromic systems - reversible photocyclization of diarylethene derivatives. *J. Org. Chem.* **1988**, *53* (4), 803−808.

(3) Neilson, B. M.; Bielawski, C. W. Illuminating Photoswitchable Catalysis. *ACS Catal.* **2013**, *3* (8), 1874−1885.

(4) Kawai, S. H.; Gilat, S. L.; Lehn, J. M. Photochemical pK(a)-modulation and gated photochromic properties of a novel diarylethene switch. *Eur. J. Org. Chem.* **1999**, *1999* (9), 2359−2366.

(5) Gostl, R.; Senf, A.; Hecht, S. Remote-controlling chemical reactions by light: Towards chemistry with high spatio-temporal resolution. *Chem. Soc. Rev.* **2014**, *43* (6), 1982−1996.

(6) Leydecker, T.; Herder, M.; Pavlica, E.; Bratina, G.; Hecht, S.; Orgiu, E.; Samori, P. Flexible non-volatile optical memory thin-film transistor device with over 256 distinct levels based on an organic bicomponent blend. *Nat. Nanotechnol.* **2016**, *11* (9), 769−775.

(7) Yildiz, I.; Deniz, E.; Raymo, F. M. Fluorescence modulation with photochromic switches in nanostructured constructs. *Chem. Soc. Rev.* **2009**, *38* (7), 1859−1867.

(8) Kim, T.; Zhu, L. Y.; Al-Kaysi, R. O.; Bardeen, C. J. Organic Photomechanical Materials. *ChemPhysChem* **2014**, *15* (3), 400−414.

(9) He, J.; Chen, F.; Liddell, P. A.; Andreasson, J.; Straight, S. D.; Gust, D.; Moore, T. A.; Moore, A. L.; Li, J.; Sankey, O. F.; Lindsay, S. M. Switching of a photochromic molecule on gold electrodes: single-molecule measurements. *Nanotechnology* **2005**, *16* (6), 695−702.

(10) Boyer, J. C.; Carling, C. J.; Gates, B. D.; Branda, N. R. Two-Way photoswitching Using One Type of Near-Infrared Light, Upconverting Nanoparticles, and Changing Only the Light Intensity. *J. Am. Chem. Soc.* **2010**, *132* (44), 15766−15772.

(11) Babii, O.; Afonin, S.; Berditsch, M.; Reisser, S.; Mykhailiuk, P. K.; Kubyshkin, V. S.; Steinbrecher, T.; Ulrich, A. S.; Komarov, I. V. Controlling Biological Activity with Light: Diarylethene- Containing Cyclic Peptidomimetics. *Angew. Chem., Int. Ed.* **2014**, *53* (13), 3392−3395.

(12) Roubinet, B.; Weber, M.; Shojaei, H.; Bates, M.; Bossi, M. L.; Beloy, V. N.; Irie, M.; Hell, S. W. Fluorescent Photoswitchable Diarylethenes for Biolabeling and Single-Molecule Localization Microscopies with Optical Superresolution. *J. Am. Chem. Soc.* **2017**, *139* (19), 6611−6620.

(13) Velema, W. A.; Szymanski, W.; Feringa, B. L. Photopharmacology: Beyond Proof of Principle. *J. Am. Chem. Soc.* **2014**, *136* (6), 2178−2191.

(14) Nakagawa, Y.; Hishida, T.; Sumaru, K.; Morishita, K.; Kirito, K.; Yokojima, S.; Sakamoto, Y.; Nakamura, S.; Uchida, K. Phototunable Cell Killing by photochromic Diarylethene of Thiazoyl and Thienyl Derivatives. *J. Med. Chem.* **2023**, *66* (8), 5937−5949.

(15) Lubbe, A. S.; Szymanski, W.; Feringa, B. L. Recent developments in reversible photoregulation of oligonucleotide structure and function. *Chem. Soc. Rev.* **2017**, *46* (4), 1052−1079.

(16) Zhang, J. J.; Zou, Q.; Tian, H. photochromic Materials: More Than Meets The Eye. *Adv. Mater.* **2013**, *25* (3), 378−399.

(17) Russew, M. M.; Hecht, S. photoswitches: From Molecules to Materials. *Adv. Mater.* **2010**, *22* (31), 3348−3360.

(18) Irie, M.; Kobatake, S.; Horichi, M. Reversible surface morphology changes of a photochromic diarylethene single crystal by photoirradiation. *Science* **2001**, *291* (5509), 1769−1772.

(19) Andreasson, J.; Pischel, U.; Straight, S. D.; Moore, T. A.; Moore, A. L.; Gust, D. All-Photonic Multifunctional Molecular Logic Device. *J. Am. Chem. Soc.* **2011**, *133* (30), 11641−11648.

(20) Andréasson, J.; Pischel, U. Light-stimulated molecular and supramolecular systems for information processing and beyond. *Coord. Chem. Rev.* **2021**, *429*, No. 213695, DOI: 10.1016/j.ccr.2020.213695.

(21) Tsivgoulis, G. M.; Lehn, J. M. Photonic molecular devices - reversibly photoswitchable fluorophores for nondestructive readout for optical memory. *Angew. Chem., Int. Ed.* **1995**, *34* (10), 1119−1122.

(22) Uno, K.; Niikura, H.; Morimoto, M.; Ishibashi, Y.; Miyasaka, H.; Irie, M. In Situ Preparation of Highly Fluorescent Dyes upon Photoirradiation. *J. Am. Chem. Soc.* **2011**, *133* (34), 13558−13564.

(23) Naren, G.; Larsson, W.; Benitez-Martin, C.; Li, S. M.; Perez-Inestrosa, E.; Albinsson, B.; Andreasson, J. Rapid amplitude-modulation of a diarylethene photoswitch: en route to contrast-enhanced fluorescence imaging. *Chem. Sci.* **2021**, *12* (20), 7073−7078.

(24) Allen, F. H. The Cambridge Structural Database: a quarter of a million crystal structures and rising. *Acta Cryst. B* **2002**, *58*, 380−388.
(25) Kawamura, I.; Kawamoto, H.; Fujimoto, Y.; Masanori, K.; Asai, K. Isomerization behavior of diarylethene-type photochromic compounds under X-ray irradiation: application to dosimetry. *Jpn. J. Appl. Phys.* **2020**, *59* (4), No. 046004.
(26) Naren, G.; Hsu, C.-W.; Li, S.; Morimoto, M.; Tang, S.; Hernando, J.; Guirado, G.; Irie, M.; Raymo, F. M.; Sundén, H.; Andréasson, J. An all-photonic full color RGB system based on molecular photoswitches. *Nat. Commun.* **2019**, *10* (1), 3996.
(27) Saha, A.; Rather, S. A.; Sharada, D.; Saha, B. K. C−X···X−C vs C−H···X−C, Which One Is the More Dominant Interaction in Crystal Packing (X = Halogen)? *Cryst. Growth Des.* **2018**, *18* (10), 6084−6090.
(28) Teyssandier, J.; Mali, K. S.; De Feyter, S. Halogen Bonding in Two-Dimensional Crystal Engineering. *ChemistryOpen* **2020**, *9* (2), 225−241.
(29) Saha, B. K.; Veluthaparambath, R. V. P.; Krishna, G. V. Halogen···Halogen Interactions: Nature, Directionality and Applications. *Chem.—Asian J.* **2023**, *18* (8), e202300067.
(30) Inoue, M.; Sumii, Y.; Shibata, N. Contribution of Organofluorine Compounds to Pharmaceuticals. *ACS Omega* **2020**, *5* (19), 10633−10640.
(31) Franke, V.; McCleaf, P.; Lindegren, K.; Ahrens, L. Efficient removal of per- and polyfluoroalkyl substances (PFASs) in drinking water treatment: nanofiltration combined with active carbon or anion exchange. *Environ. Sci. Water Res. Technol.* **2019**, *5* (11), 1836−1843.
(32) Nikolayenko, V. I.; Castell, D. C.; van Heerden, D. P.; Barbour, L. J. Guest-Induced Structural Transformations in a Porous Halogen-Bonded Framework. *Angew. Chem., Int. Ed.* **2018**, *57* (37), 12086−12091.
(33) Sobczak, S.; Półrolniczak, A.; Ratajczyk, P.; Cai, W.; Gładysiak, A.; Nikolayenko, V. I.; Castell, D. C.; Barbour, L. J.; Katrusiak, A. Large negative linear compressibility of a porous molecular co-crystal. *Chem. Commun.* **2020**, *56* (31), 4324−4327.
(34) Priimagi, A.; Cavallo, G.; Forni, A.; Gorynsztejn−Leben, M.; Kaivola, M.; Metrangolo, P.; Milani, R.; Shishido, A.; Pilati, T.; Resnati, G.; Terraneo, G. Halogen Bonding versus Hydrogen Bonding in Driving Self-Assembly and Performance of Light-Responsive Supramolecular Polymers. *Adv. Funct. Mater.* **2012**, *22* (12), 2572−2579.
(35) Priimagi, A.; Saccone, M.; Cavallo, G.; Shishido, A.; Pilati, T.; Metrangolo, P.; Resnati, G. Photoalignment and Surface-Relief-Grating Formation are Efficiently Combined in Low-Molecular-Weight Halogen-Bonded Complexes. *Adv. Mater.* **2012**, *24* (44), OP345−OP352.
(36) *CrysAlis PRO, V1.171.42.79a*; Rigaku Oxford Diffraction: 2022.
(37) Sheldrick, G. SHELXT - Integrated space-group and crystal-structure determination. *Acta Cryst. A* **2015**, *71* (1), 3−8.
(38) Bondi, A. van der Waals Volumes and Radii. *J. Phys. Chem.* **1964**, *68* (3), 441−451.
(39) Fujimoto, A.; Fujinaga, N.; Nishimura, R.; Hatano, E.; Kono, L.; Nagai, A.; Sekine, A.; Hattori, Y.; Kojima, Y.; Yasuda, N.; Morimoto, M.; Yokojima, S.; Nakamura, S.; Feringa, B. L.; Uchida, K. Photoinduced swing of a diarylethene thin broad sword shaped crystal: a study on the detailed mechanism. *Chem. Sci.* **2020**, *11* (45), 12307−12315.
(40) Cavallo, G.; Metrangolo, P.; Milani, R.; Pilati, T.; Priimagi, A.; Resnati, G.; Terraneo, G. The Halogen Bond. *Chem. Rev.* **2016**, *116* (4), 2478−2601.
(41) Öhrström, L. Designing, Describing and Disseminating New Materials by using the Network Topology Approach. *Chem.—Eur. J.* **2016**, *22* (39), 13758−13763.
(42) Johnson, M. T.; Dzolic, Z.; Cetina, M.; Wendt, O. F.; Öhrström, L.; Rissanen, K. Neutral Organometallic Halogen Bond Acceptors: Halogen Bonding in Complexes of PCPPdX (X = Cl, Br, I) with Iodine (I(2)), 1,4-Diiodotetrafluorobenzene (F4DIBz), and 1,4-Diiodooctafluorobutane (F8DIBu). *Cryst. Growth & Design* **2012**, *12* (1), 362−368.
(43) Schoedel, A.; Li, M.; Li, D.; O'Keeffe, M.; Yaghi, O. M. Structures of Metal-Organic Frameworks with Rod Secondary Building Units. *Chem. Rev.* **2016**, *116* (19), 12466−12535.
(44) Mukherjee, A.; Tothadi, S.; Desiraju, G. R. Halogen Bonds in Crystal Engineering: Like Hydrogen Bonds yet Different. *Acc. Chem. Res.* **2014**, *47* (8), 2514−2524.
(45) Xie, L. S.; Alexandrov, E. V.; Skorupskii, G.; Proserpio, D. M.; Dincă, M. Diverse $\pi-\pi$ stacking motifs modulate electrical conductivity in tetrathiafulvalene-based metal−organic frameworks. *Chem. Sci.* **2019**, *10* (37), 8558−8565.
(46) Tshuma, P.; Makhubela, B. C. E.; Öhrström, L.; Bourne, S. A.; Chatterjee, N.; Beas, I. N.; Darkwa, J.; Mehlana, G. Cyclometalation of lanthanum(iii) based MOF for catalytic hydrogenation of carbon dioxide to formate. *RSC Adv.* **2020**, *10* (6), 3593−3605.
(47) Amombo Noa, F. M.; Abrahamsson, M.; Ahlberg, E.; Cheung, O.; Göb, C. R.; McKenzie, C. J.; Öhrström, L. A unified topology approach to dot-, rod-, and sheet-MOFs. *Chem.* **2021**, *7* (9), 2491−2512.
(48) Delgado-Friedrichs, O.; Hyde, S. T.; O'Keeffe, M.; Yaghi, O. M. Crystal structures as periodic graphs: the topological genome and graph databases. *Struct. Chem.* **2017**, *28* (1), 39−44.
(49) Spackman, M. A.; Jayatilaka, D. Hirshfeld surface analysis. *CrystEngComm* **2009**, *11* (1), 19−32.
(50) Jelsch, C.; Ejsmont, K.; Huder, L. The enrichment ratio of atomic contacts in crystals, an indicator derived from the Hirshfeld surface analysis. *IUCrJ.* **2014**, *1* (2), 119−128.

Recommended by ACS

Photophysical Behavior of Triethylmethylammonium Tetrabromoferrate(III) under High Pressure
Takeshi Nakagawa, Martina Vrankić, *et al.*
NOVEMBER 21, 2023
INORGANIC CHEMISTRY
READ

Partial Proton Transfer in the Gas Phase: A Spectroscopic and Computational Analysis of the Trifluoroacetic Acid – Trimethylamine Complex
Aaron J. Reynolds and Kenneth R. Leopold
DECEMBER 11, 2023
THE JOURNAL OF PHYSICAL CHEMISTRY A
READ

Spin Coupling Effect on Geometry-Dependent X-Ray Absorption of Diradicals
Scott M. Garner, Eric Neuscamman, *et al.*
JANUARY 18, 2024
JOURNAL OF THE AMERICAN CHEMICAL SOCIETY
READ

Lattice Dynamics of Quinacridone Polymorphs: A Combined Raman and Computational Approach
Andrea Giunchi, Alberto Girlando, *et al.*
JULY 31, 2023
CRYSTAL GROWTH & DESIGN
READ

Get More Suggestions >

https://doi.org/10.1021/acs.cgd.3c00767
Cryst. Growth Des. 2024, 24, 923−931